Local electronic state in the high-valence hollandite-type chromium oxide $K_2Cr_8O_{16}$ investigated by ^{53}Cr NMR

Hikaru Takeda,[1] Yasuhiro Shimizu,[1] Masayuki Itoh,[1] Masahiko Isobe,[2] and Yutaka Ueda[2]
[1]*Department of Physics, Graduate School of Science, Nagoya University, Furo-cho, Chikusa-ku, Nagoya 464-8602, Japan*
[2]*Institute for Solid State Physics, University of Tokyo, Kashiwanoha, Kashiwa 277-8581, Japan*
(Received 17 July 2013; published 4 October 2013)

We have performed ^{53}Cr NMR measurements to investigate the local electronic state of a hollandite-type chromium oxide $K_2Cr_8O_{16}$ which undergoes an unusual metal-insulator (MI) transition at $T_{MI} = 95$ K in the ferromagnetic phase. In the ferromagnetic insulating phase, we observed NMR spectra with internal fields different from each other at the four Cr sites. From an analysis of the hyperfine fields, the difference in the isotropic internal field is related to the supertransferred hyperfine (STH) field. The slight difference in the electron occupation of the 3*d* orbital at the four Cr sites is detected through the different STH field governed by the different charge-transfer passes. The presence of the STH field shows the strong hybridization of the chromium 3*d* orbitals and oxygen 2*p* orbital which leads to the characteristic MI transition.

DOI: 10.1103/PhysRevB.88.165107 PACS number(s): 71.30.+h, 75.50.Cc, 76.60.−k, 75.60.Ch

I. INTRODUCTION

The 3*d* transition-metal oxides in the charge-transfer (CT) region have been of great interest due to peculiar phenomena such as high-temperature superconductivity, colossal magnetoresistance, and spin-state transition.[1,2] The origins of these phenomena are closely related to electronic states resulting from strong hybridization between the oxygen 2*p* orbital and 3*d* orbital of the transition-metal ions. Especially in the high-valence oxides an intriguing electronic state appears due to the small or negative charge-transfer energy.[2] Chromium oxides have recently attracted special attention as one such system. In these oxides, some Cr t_{2g} orbitals hybridize with O 2*p* orbitals and form dispersive bands with itinerant character, while the other t_{2g} orbitals form relatively dispersionless bands.[3–5] Then an orbital selective Mott insulating state is realized and provides us rich physics.[6] Indeed, a low-valence oxide $Cr^{3+}{}_2O_3$ in the Mott-Hubbard region is a conventional Mott insulator,[7] whereas a high-valence oxide $Cr^{4+}O_2$ in the CT region is a ferromagnetic (FM) half metal caused by the double exchange mechanism.[3]

Among the high-valence Cr oxides, intensive studies have been devoted to the calcium-ferrite-type oxide $NaCr^{3.5+}{}_2O_4$ and the hollandite-type one $K_2Cr^{3.75+}{}_8O_{16}$ with frustrated quasi-one-dimensional (quasi-1D) lattices formed by double chains.[5,8–16] The quasi-1D structure and geometrical frustration play important roles for their magnetism and transport properties in addition to CT. $NaCr_2O_4$, an antiferromagnetic (AFM) insulator, exhibits a new type of colossal magnetoresistance (CMR) at the AFM phase,[8–10] which is different from a conventional CMR in the FM compounds such as manganites.[17] This phenomenon is discussed on the basis of the CT processes between Cr and O ions and the geometrical frustration which make the magnetically ordered state instable.[8,10] On the other hand, $K_2Cr_8O_{16}$ is an FM half metal with the Curie temperature $T_C = 180$ K and undergoes the metal-insulator (MI) transition at $T_{MI} = 95$ K in the FM state.[13] Just after the discovery of the MI transition, several scenarios based on the orbital or charge ordering (CO)[13,14] and the charge-density wave (CDW)[5] were proposed to explain the MI transition. However, insufficient information on the crystal structure prevented us from clarifying which scenario is the most suitable. More recently Nakao *et al.* demonstrated from synchrotron x-ray-diffraction experiments that the MI transition is accompanied by a structural transition from the tetragonal $I4/m$ to monoclinic $P112_1/a$ phases.[15] Below T_{MI}, one Cr site splits into four crystallographically inequivalent sites, which form two kinds of uniform double chains composed of Cr2 and Cr4 sites and an alternating double chain with Cr1 and Cr3 sites, as shown in Fig. 1. Furthermore Toriyama *et al.* proposed from electronic structure calculations with local-density approximation and generalized gradient approximation (GGA) methods that the MI transition is driven by a Peierls instability in the quasi-1D column composed of the four Cr–O chains.[16] In their scenario, chromium 3*d* orbitals strongly hybridize with oxygen 2*p* orbitals and the charge densities are almost the same at all the chromium ions even though $K_2Cr_8O_{16}$ is a Peierls insulator. It is desired to experimentally clarify the actual local electronic state via a microscopic probe.

In this study, we have performed ^{53}Cr nuclear magnetic resonance (NMR) measurements on a powder sample to clarify the local electronic state of $K_2Cr_8O_{16}$. In the ferromagnetic insulating phase, we observe the NMR signals from domain walls in zero field and from domains in a magnetic field above 5 kOe. Both signals form powder patterns composed of four NMR spectra coming from the four crystallographically inequivalent Cr sites. In spite of uniform charge densities at all the Cr sites the internal fields at the Cr sites differ from each other. We discuss the origin of such difference in the internal field from the analysis based on the on-site hyperfine field and the supertransferred (STH) one. Owing to the slight difference in the orbital occupation of 3*d* electrons at the four Cr sites, there may appear different charge-transfer passes and STH fields. This is a peculiar feature in the negative CT compounds.

II. EXPERIMENTAL PROCEDURE

Sintered polycrystalline samples of $K_2Cr_8O_{16}$ were prepared by solid-state reaction of a mixture with the ratio of $K_2Cr_2O_7 : Cr_2O_3 = 1 : 3$ under 6.7 GPa at 1273 K for

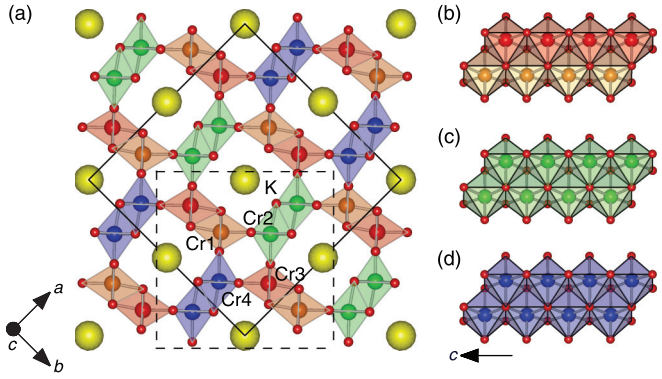

FIG. 1. (Color online) (a) Crystal structure of the insulating phase of $K_2Cr_8O_{16}$, which was determined from the synchrotron x-ray-diffraction experiment [Ref. 15], projected on the *ab* plane. The solid parallelogram represents a unit cell, whereas the dashed square is a unit for the analysis of the supertransferred hyperfine field [see Fig. 7(b)]. (b)–(d) Three kinds of edge-shared double chains in $K_2Cr_8O_{16}$.

1 h.[13] In the present NMR measurements we used several samples having a nearly spherical shape with a diameter of ∼2 mm. The ^{53}Cr NMR measurements were performed using a coherent pulsed spectrometer and a superconducting magnet. The frequency-swept NMR spectra were taken point by point in magnetic fields of $H = 0$, 1.5, 3, 5, 20, and 30 kOe. We also performed ^{53}Cr NMR measurements on CrO_2, Cr_2O_3, and $YCrO_3$ as reference materials. Polycrystalline samples of CrO_2 and Cr_2O_3 used in the NMR measurements are commercial products, whereas $YCrO_3$ was prepared by a conventional solid-state reaction method.[18]

Since the results in the next section are obtained from analyzing NMR spectra, it will be useful to present characteristic features of NMR signals and spectra in a ferromagnetic polycrystalline sample. In the FM state, spontaneous magnetic moments generate the internal field $\mathbf{H}_n$, which is composed of the hyperfine, classical dipole, demagnetization, and Lorentz fields.[19] The NMR frequency ν is expressed as

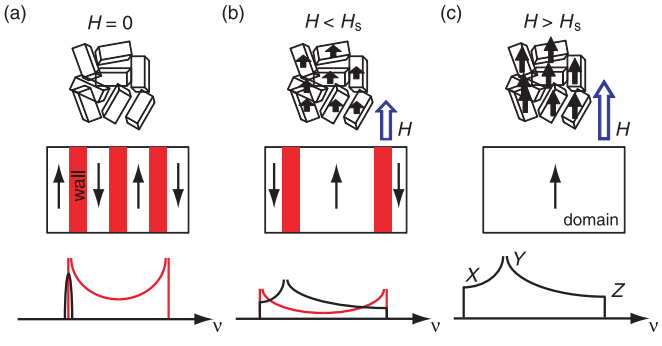

FIG. 2. (Color online) Schematic representations of magnetization, domain and domain walls, and NMR spectra in a ferromagnetic polycrystalline sample (a) at zero field, (b) below H_s, and (c) above H_s, where H_s is the magnetic field above which magnetization saturates. The NMR spectra from magnetic domains and walls are represented by the black and red curves, respectively. A divergence or step in the powder pattern appears at singularity points for $H_n \| k$ where the k (X, Y, and Z) axes are the local symmetry ones defined in the text.

$\nu = \gamma|\mathbf{H}_n + \mathbf{H}|/2\pi$, where γ (equal to $2\pi \times 2.4065$ MHz/T for ^{53}Cr) is the nuclear gyromagnetic ratio and the external magnetic field $\mathbf{H}$ is included. At zero external field one can detect NMR signals from nuclei located in magnetic domains and domain walls. The domain signals are observed as a relatively narrow spectrum dependent on the multidomain structure, whereas the domain-wall ones show a so-called powder pattern. If H_n, which is governed by the hyperfine field, is almost contentiously rotated in a plane, where the domain walls exist, by the rotation of the wall moments, its anisotropy leads to a two-dimensional (2D) powder pattern, as schematically presented in Fig. 2(a). Then it can be calculated by taking summation over 2D random orientation of the resonance condition $\nu = \gamma|\mathbf{H}_n|/2\pi$ relative to $\mathbf{H}_n$. Also, the domain-wall signals have a signal enhancement effect with an enhancement factor $\eta = 10^2$–10^4,[20] which enables us to easily observe the NMR signals from the nuclei with a small natural abundance such as ^{53}Cr (9.55%),[21,22] ^{57}Fe (2.19%),[23] and ^{61}Ni (1.19%).[24] With application of an external magnetic field, the domain walls are partially removed and magnetization increases, resulting in the evolution of the powder pattern dependent on the inhomogeneous distribution of magnetization due to the domain structure, as schematically depicted in Fig. 2(b). Above H_s, where magnetization saturates and the local magnetic moment $\mathbf{M}$ becomes parallel to $\mathbf{H}$, the sample sets in a single domain state. Then we can take more quantitative treatment of the NMR spectrum than we can below H_s. The internal field is effectively written as $\mathbf{H}_n = \mathbf{A}_{eff}\mathbf{M}$ with a coupling tensor $\mathbf{A}_{eff}$. For a polycrystalline sample, one can observe only a domain spectrum having a three-dimensional (3D) powder pattern similar to that in a paramagnetic phase,[25] as shown in Fig. 2(c). The powder pattern can be calculated by taking summation over 3D random orientation of the resonance condition $\nu = \gamma|\mathbf{H}_n + \mathbf{H}|/2\pi$ relative to $\mathbf{H}$. It is characterized by H_n^k ($k = X, Y, Z$), which are the internal fields for $H_n \| k$ in the XYZ coordinate system where the $\mathbf{A}_{eff}$ tensor is diagonalized. Then a divergence or step appears at $\nu = \gamma|H_n^k + H|/2\pi$, as schematically presented in Fig. 2(c). When the hyperfine field is much larger than the others, the $\mathbf{A}_{eff}$ tensor is governed by the hyperfine coupling one. We define the isotropic internal field as $H_n^{iso} = (H_n^X + H_n^Y + H_n^Z)/3$, the axially anisotropic one as $H_n^{ax} = (2H_n^Z - H_n^X - H_n^Y)/6$, and the in-plane anisotropic one as $H_n^{aniso} = (H_n^Y - H_n^X)/2$, which are useful for discussion on the origin of H_n and electronic states in Sec. V. It should be also noted that the demagnetization field in a spherical sample is canceled by the Lorentz field. Then H_n^{iso} comes from the hyperfine field, whereas the hyperfine field and the classical dipole field $\mathbf{H}_D$ contribute to H_n^{ax} and H_n^{aniso}.

III. EXPERIMENTAL RESULTS AND ANALYSIS

Figure 3(a) shows the frequency-swept ^{53}Cr NMR spectrum with $\eta \sim 200$, which was determined by comparing the optimal pulse width with that of ^{1}H NMR, in $K_2Cr_8O_{16}$ at 0 kOe and 4.2 K. Several peaks are seen except two small peaks located at 26.5 and 37.2 MHz coming from an impurity CrO_2.[21,22] In general, an NMR spectrum is governed by the magnetic and electric interactions. The splitting of the observed peaks at ∼5 MHz is too large to be explained by the quadrupole splitting with the electric quadrupole frequency ν_Q, which is less than

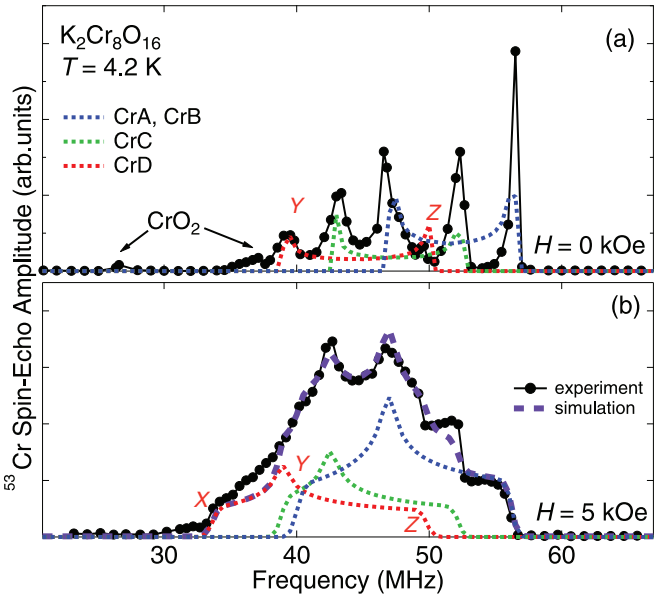

FIG. 3. (Color online) ^{53}Cr NMR spectra in an external magnetic field of (a) $H = 0$ kOe and (b) $H = 5$ kOe at 4.2 K for $K_2Cr_8O_{16}$. The solid lines are guide to the eye. The color dotted curves with the symbols CrA-CrD are numerically calculated spectra by assuming the internal fields presented in Table I and the two-dimensional (three-dimensional) powder patterns in the upper (lower) figure. The purple dashed curve is the summation of the four spectra. A peak or step in the powder patterns appears at singularity points for $H_n \| k$, where the k (X, Y, and Z) axes are the local symmetry ones defined in the text.

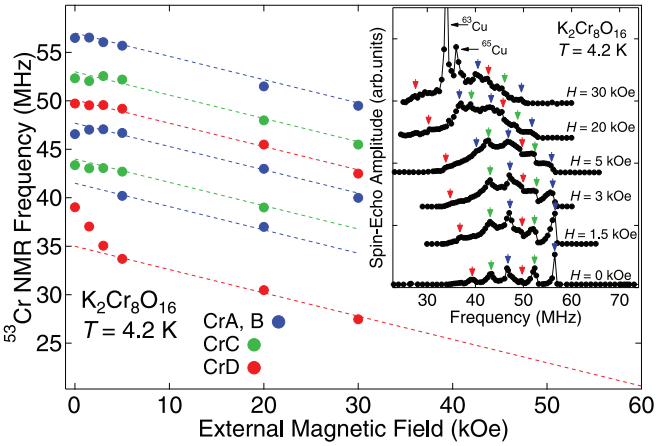

FIG. 4. (Color online) External field dependence of the NMR frequency at the singularity point of the ^{53}Cr NMR spectra at 4.2 K in $K_2Cr_8O_{16}$. The dashed lines have the slope $-\gamma/2\pi$, where γ is the nuclear ^{53}Cr gyromagnetic ratio. Inset: NMR spectra at various fields and 4.2 K with the singularity points presented by the arrows. The ^{63,65}Cu NMR spectra come from a copper NMR coil.

$\sim$1 MHz, reported for several chromium compounds.[26,27] Thus the observed NMR spectrum should be explained by the magnetic interaction. As seen in Fig. 2(a), a domain-wall spectrum is expected to show a powder pattern even at zero magnetic field. The zero-field NMR spectrum is reasonably reproduced by the summation of the four 2D powder patterns denoted by the symbols CrA–CrD from the nuclei of four kinds of Cr sites in domain walls, as seen in Fig. 3(a). The color dotted curves in Fig. 3(a) represent the calculated spectra, which are calculated numerically for the internal fields listed in Table I and convoluted by the Gaussian with the width of 0.3 MHz, by assuming that the direction of the internal fields is randomly distributed in the YZ plane where the domain walls exist. In each 2D powder pattern two peaks appear at $\nu = \gamma|H_n^k|/2\pi$ ($k = Y$ and Z), as shown in Fig. 3(a).

Magnetization saturates and becomes parallel to H above $H_s \sim 5$ kOe where the sample sets in a single domain state at 4.2 K. Then we can observe the domain spectrum with the 3D powder pattern, as seen in Fig. 2(c). Figure 3(b) shows the ^{53}Cr frequency-swept NMR spectrum at 5 kOe and 4.2 K. This spectrum is well reproduced by the purple dashed spectrum, which is the summation of four 3D powder patterns CrA–CrD calculated by assuming the single domain and the internal fields listed in Table I. In each 3D powder pattern two steps appear at $\nu = \gamma|H_n^k + H|/2\pi$ ($k = X$ and Z) and the Y singularity leads to a peak at $\nu = \gamma|H_n^Y + H|/2\pi$, as shown in Fig. 3(b). Thus both the domain and domain-wall spectra are reproduced by the four CrA–CrD spectra, consistent with the four crystallographically inequivalent Cr sites reported by the x-ray-scattering measurements.[15,16] Also, the experimental result that the CrA and CrB spectra have the same parameters of H_n shows the presence of two Cr sites with electronic states similar to each other. This seems to be related to the type of the double chain, the uniform or alternating one. The two sites may be the Cr2 and Cr4 ones in the uniform double chains; otherwise they are the Cr1 and Cr3 ones in the alternating double chain.

TABLE I. The isotropic internal field H_n^{iso}, the axially anisotropic one H_n^{ax}, and the in-plane anisotropic one H_n^{aniso} of the four Cr sites, which lead to the CrA–CrD spectra, at 4.2 K in the ferromagnetic insulating phase of $K_2Cr_8O_{16}$.

Spectrum	H_n^{iso} (kOe)	H_n^{ax} (kOe)	H_n^{aniso} (kOe)
CrA	−203	−17.7	−14.4
CrB	−203	−17.7	−14.4
CrC	−190	−15.9	−7.7
CrD	−175	−18.8	−11.1

The spectrum changes from the 2D to the 3D powder patterns with increasing H below H_s, as seen in the inset of Fig. 4. This is related to the disappearance of the domain walls in the external magnetic field, as seen in Fig. 2(b). The NMR frequencies where the spectrum shows singularities are plotted against H in Fig. 4. This is clearly demonstrated by the change in the lowest singularity of the CrD spectrum. A new singularity appears below the Y singularity of the domain-wall spectrum at zero field with applying H and moves to the X singularity in the single-domain spectrum at $\sim$5 kOe with increasing H. Above $\sim$5 kOe, the NMR frequency ν follows the resonance condition $\nu = \gamma(H_0 - H)/2\pi$ with a constant H_0. This means that the NMR spectrum comes from the Cr nuclei in the single domain above $\sim$5 kOe.

With increasing temperature T, the internal magnetic field H_n gradually decreases. Figure 5 shows the T dependence of the normalized internal field $H_n^Z(T)/H_n^Z(0)$ for the CrA–CrC spectra in $K_2Cr_8O_{16}$. Then it follows the relation $H_n^Z(T)/H_n^Z(0) = 1 - a_0 T^{3/2}$ with $|H_n^Z(0)| = 194(179)$ kOe

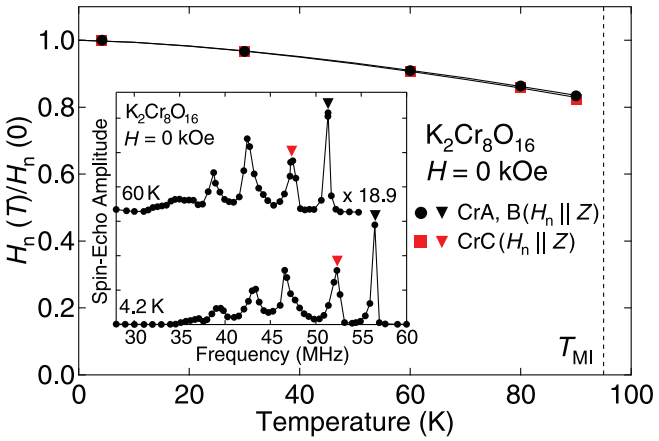

FIG. 5. (Color online) Temperature dependence of $H_n^Z(T)/H_n^Z(0)$ for the CrA–CrC spectra in the ferromagnetic insulating phase of $K_2Cr_8O_{16}$. Inset: Zero-field ^{53}Cr NMR spectra with the inverted triangles, which denote the NMR frequencies for $H_n \| Z$, at 4.2 and 60 K. The solid curves represent the fitted results of the data to the relation $H_n^Z(T)/H_n^Z(0) = 1 - a_0 T^{3/2}$.

and $a_0 \times 10^4 = 1.93\ (2.00)\ \mathrm{K}^{-3/2}$ for CrA–CrB (CrC), which is governed by the 3D FM spin-wave excitation.[28] It should be also noted that H_n, which is proportional to spontaneous magnetization, decreases toward not T_{MI}, where the MI transition takes place accompanied by the structural transition, but T_C. This is consistent with the T dependence of bulk magnetization.[13] The poor signal-to-noise ratio prevented us from observing a precise NMR spectrum above T_{MI}.

For comparing $K_2Cr_8O_{16}$ with other Cr oxides, ^{53}Cr NMR spectra of the FM half metal CrO_2 and insulating antiferromagnets Cr_2O_3 and $YCrO_3$ at zero external field and 4.2 K are presented in Fig. 6. The NMR spectra with a strong signal enhancement are located at 26.50 and 37.19 MHz, which are consistent with reported data,[21,22] in CrO_2. In the NMR spectrum of Cr_2O_3 the centerline at 70.23 MHz, as reported in Ref. 29, is accompanied by two satellites with the frequency splitting $\delta\nu \sim 0.27$ MHz governed by the nuclear quadrupole interaction and the internal field due to the AFM moments. Also a similar spectrum with $\delta\nu \sim 0.50$ MHz is observed at 68.74 MHz, as reported in Ref. 27, in $YCrO_3$.

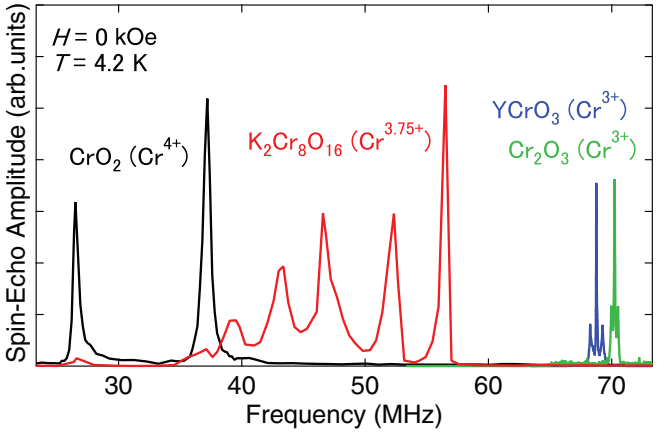

FIG. 6. (Color online) ^{53}Cr NMR spectra of CrO_2, $K_2Cr_8O_{16}$, Cr_2O_3, and $YCrO_3$ at zero external field and 4.2 K.

IV. DISCUSSION

The present NMR results, particularly the hyperfine fields, are expected to provide information on the electronic state related to the mechanism of the MI transition in $K_2Cr_8O_{16}$ such as CO,[14] CDW,[5] and the Peierls instability[16] in the quasi-1D column composed of the four Cr–O chains.

In Table I, it should be noted that there is the difference in H_n^{iso} at the four Cr sites of $K_2Cr_8O_{16}$. One possible origin of the difference is CO. The NMR spectrum is closely related to the valence of the Cr ion via the hyperfine field. As seen in Fig. 6, the ^{53}Cr NMR spectrum in the tetravalent Cr oxide CrO_2 is located at 26–37 MHz, whereas the spectra are observed around 70 MHz for the trivalent ones Cr_2O_3 and $YCrO_3$. The fact that the spectrum of $K_2Cr_8O_{16}$ is located at the intermediate frequencies between those of the trivalent and tetravalent Cr oxides excludes the scenario of CO into Cr^{3+} and Cr^{4+} sites below T_{MI} in $K_2Cr_8O_{16}$. Another possible origin is CDW.[5] On the assumption of the same isotropic hyperfine coupling constant at the four Cr sites in $K_2Cr_8O_{16}$, spontaneous magnetic moments of CrA–CrB, CrC, and CrD are obtained from the H_n^{iso} data listed in Table I as $2.37\mu_B$, $2.19\mu_B$, and $2.07\mu_B$, respectively. Here it should be noted that H_n^{iso} is governed by the microscopic hyperfine field, because the demagnetization field is almost canceled by the Lorentz field due to the nearly spherical shape of the samples. Since the magnetic moments are fully polarized, these spontaneous magnetic moments may be proportional to the charge densities. Then the difference in the charge density among the four Cr sites is expected to be ~0.3 electrons/Cr, inconsistent with the result of the valence bond sum calculation of less than ~0.03 electrons/Cr.[16] Thus we should search for other origins. In transition-metal oxides belonging to the CT region such as high-temperature superconducting cuprates, the $3d$ orbitals strongly hybridize with the O $2p$ orbitals and consequently an anomalous hyperfine field appears via the spin transfer processes.[30,31] In $K_2Cr_8O_{16}$ this transferred hyperfine field from the neighboring Cr sites may contribute to H_n^{iso} at the four Cr sites in addition to the on-site hyperfine interaction, as will be discussed below.

In general, the hyperfine interaction between a nucleus and on-site electrons in the $3d$ electron systems is expressed as $\mathcal{H} = \sum_i 2\mu_B \gamma \hbar \mathbf{s}_i \cdot \mathbf{A}_i \cdot \mathbf{I}$, with Plank's constant $\hbar$, the nuclear spin operator $\mathbf{I}$, Bohr magneton μ_B, and the ith electron's spin operator $\mathbf{s}_i$ and hyperfine coupling constant $\mathbf{A}_i$. Then the spin-orbit hyperfine interaction may be neglected due to the small spin-orbit parameter in the light transition-metal ions.[32–38] Indeed, the g value of ~1.98 reported for CrO_2 with the electronic state similar to that of $K_2Cr_8O_{16}$ indicates that the spin-orbit effect may be small in the high-valence Cr oxides.[37] Thus $\mathbf{A}_i$ is further expressed as $\mathbf{A}_i = -(\kappa \mathbf{1} + \frac{2}{21}\mathbf{q}_i)\langle r^{-3}\rangle$, with a parameter of the Fermi contact interaction κ, the quadrupole moment tensor $q_{\alpha\beta} = \frac{3}{2}(l_\alpha l_\beta + l_\beta l_\alpha) - \delta_{\alpha\beta} l^2$ with the orbital momentum l, and $\langle r^{-3}\rangle$ being the expectation value of r^{-3} for the $3d$ orbitals.[38,39] The first term of $\mathbf{A}_i$ due to the core polarization of inner s spins generates an isotropic Fermi contact field $\mathbf{H}_{cp}$, whereas the second term leads to a dipole hyperfine field $\mathbf{H}_{dip}$ which mainly contributes to the on-site anisotropic field. On the other hand, the transferred hyperfine interaction arises via several kinds of spin transfer

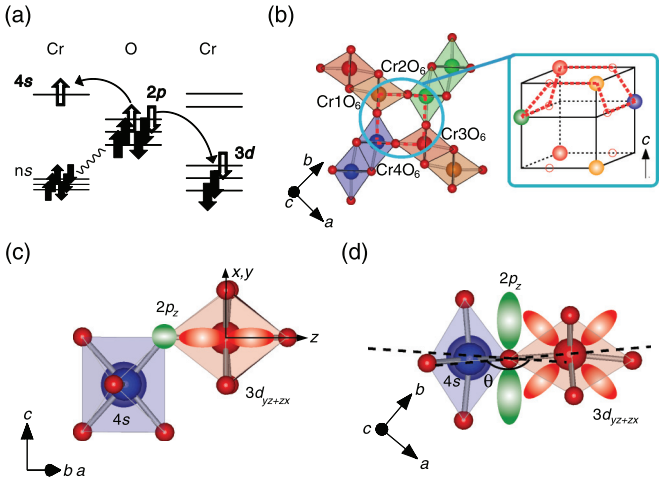

FIG. 7. (Color online) (a) Schematic representations of the spin transfer process from the Cr-3d to Cr-4s orbitals via the oxygen 2p orbital and the overlap of the Cr ns (n = 1–3) orbitals and the oxygen 2p orbital. (b) The Cr_8O_{16} network, the dashed square in Fig. 1(a), projected on the ab plane and the four chain column depicted schematically in the insulating phase of $K_2Cr_8O_{16}$. The corner-shared CrO_6 of Cr3 and Cr4 with the Cr 4s and $3d_{yz+zx}$ orbitals and the oxygen $2p_z$ orbital projected on (c) the plane including the c axis and (d) the ab plane.

processes from the neighboring magnetic sites. One of them is a supertransfer process leading to the supertransferred hyperfine (STH) field $\mathbf{H}_{\rm STH}$.[40] In this process, a magnetic cation first polarizes the p electrons of the anion ligand, and then the spin-polarized electrons of the ligand transfer to the neighboring metal 4s orbital or polarize the metal core (1s–3s) electron by an overlap effect between the polarized ligand and the core electrons, creating an isotropic magnetic field at the cation site due to the Fermi contact interaction, as depicted in Fig. 7(a). The other spin transfer process is what is called the exchange polarization process.[41] In the transition-metal compounds having only t_{2g} electrons, the ligand $p\sigma$ electrons can be polarized by the virtual spin transfer to the unoccupied e_g orbitals at the metal site, inducing an isotropic magnetic field in the same way as mentioned in the supertransfer process. However, this process may have a small contribution to the isotropic internal field due to small spin transfer through the hybridization between these orbitals.[42]

In $K_2Cr_8O_{16}$, a Cr site is surrounded by eight neighboring Cr sites, leading to the eight transfer paths. Among them, the effect of six paths may be neglected, because the STH process via the four paths in the double chain does not appear due to no hybridization between the Cr 3d and O 2p orbitals, and also the other two paths in the quasi-1D column composed of the four-CrO chains are not active due to the bond alternation along the c axis.[15,16] Thus we should consider only two Cr–O–Cr paths, as depicted with the dashed lines in Fig. 7(b), to evaluate the transferred field. The STH field is written as $\mathbf{H}_{\rm STH} = \sum_{k=1}^{2} \mathbf{B}_k \cdot \mathbf{M}_k$ with the supertransferred coupling tensor $\mathbf{B}_k$ from magnetic moments $\mathbf{M}_k$ at the two Cr sites. It should be noted that the STH process mentioned above results in an isotropic field.

In a microscopic point of view, $H_{\rm STH}$ can be governed by some parameters such as overlap integral of the wave functions, covalence parameters, and bonding angles, as discussed in the theoretical and experimental studies on $H_{\rm STH}$.[43–45] In $K_2Cr_8O_{16}$, the partial $H_{\rm STH}$ at the Cr4 site generated by a neighboring Cr3 site may be expressed as

$$H_{\rm STH} \propto \left\{ -\sum_{n=1}^{3} s_{\rm ns}\phi_{\rm ns}(0) + b_{4s}\phi_{4s}(0) \right\}^2 \times \left\{ \left[a_{yz+zx}^{\uparrow 2} - a_{yz+zx}^{\downarrow 2} \right] \sin^2\theta \right\}, \quad (1)$$

taking account of the transfer path, as depicted in Figs. 7(c) and 7(d). Here, $s_{ns} = \langle p_z \mid ns \rangle$ are the pair overlap integrals of the Cr ns (n = 1–3) orbitals with the oxygen 2p orbital in the Cr–O bond, $\phi_{\rm ns}(0)$ is the wave function of the electrons in the ns orbital of Cr ions, b_{4s} is the covalency parameter describing the electron transfer from the oxygen 2p orbital into an empty Cr 4s orbital, $a_{yz+zx}^{\uparrow(\downarrow)}$ is the covalence parameter for d_{yz+zx}-p_z which depends on the direction of the Cr spin, and θ is the angle in Cr–O–Cr projected into the ab plane. Here we introduce the x, y, and z axes, which may be parallel to the $X-Y$, $X+Y$, and Z direction, respectively, as local axes depicted in Fig. 7(c) to use the description of the t_{2g} orbital in the theoretical studies.[5,16] Then the value of $H_{\rm STH}$ strongly depends on the covalence parameter between d_{yz+zx} and p_z orbitals and the Cr–O–Cr bonding angle. Since this covalence parameter is expected to be large due to the strong d-p orbital hybridization and θ is not completely π, $H_{\rm STH}$ may arise through this transfer path. Also, other transfer processes via Cr(e_g)-O(p_σ)-Cr(s) or Cr(d_{yz-zx})-O(p_x)-Cr(s), which are not usually active because of cubic lattice symmetry at the Cr sites or weak d-p hybridization, may contribute to $H_{\rm STH}$. Thus the supertransferred hyperfine coupling constant B, which is isotropic, such as $B = +14.6$ kOe/$\mu_{\rm B}$ for $LaVO_3$ ($3d^2$, Ref. 42) and $+45.8$ kOe/$\mu_{\rm B}$ for $YB_2Cu_3O_{7-\delta}$ ($3d^9$, Ref. 31), can be present in $K_2Cr_8O_{16}$ ($3d^{2.25}$), although it cannot be determined in the present experiment.

From the discussion above, the internal field in $K_2Cr_8O_{16}$ can be expressed as $\mathbf{H}_{\rm n} = \mathbf{H}_{\rm cp} + \mathbf{H}_{\rm dip} + \mathbf{H}_{\rm STH} + \mathbf{H}_{\rm D}$. It should be again noted that the demagnetization field and the Lorentz one are negligible due to their cancellation in the nearly spherical samples. The classical dipole field $\mathbf{H}_{\rm D}$ is evaluated as $H_{\rm D}^{\rm ax} = -1.67$ and $H_{\rm D}^{\rm aniso} = -0.24$ kOe, where the definitions of $H_{\rm D}^{\rm ax}$ and $H_{\rm D}^{\rm aniso}$, respectively, follow those of $H_{\rm n}^{\rm ax}$ and $H_{\rm n}^{\rm aniso}$, for the Cr1–Cr4 sites by taking summation over the lattice points with the spontaneous moment of $M = 2.25\mu_{\rm B}$ in the Lorentz sphere. From the $H_{\rm n}$ values listed in Table I, we evaluate the electron occupation number n_j (equal to $2.25 f_j$ with the fraction of the electron number f_j and $\sum_j f_j = 1$) of the d_j ($j = xy$, $yz \pm zx$) orbital. Since the t_{2g} electrons are fully polarized in the FM phase of $K_2Cr_8O_{16}$,[5,13,16] the dipole hyperfine field $\mathbf{H}_{\rm dip}$ can be decomposed as[35,36,38] $\mathbf{H}_{\rm dip} = -\sum_j \frac{2}{21} \langle r^{-3} \rangle f_j \mathbf{q}_j \cdot \mathbf{M}$. Therefore, $H_{\rm dip}^{\rm ax}$ and $H_{\rm dip}^{\rm aniso}$, which are defined by the equations similar to $H_{\rm n}^{\rm ax}$ and $H_{\rm n}^{\rm aniso}$ in Sec. III, are written by $H_{\rm dip}^{\rm ax} = \frac{1}{7} M \langle r^{-3} \rangle (f_{yz+zx} + f_{yz-zx} - 2f_{xy})$ and $H_{\rm dip}^{\rm aniso} = \frac{3}{7} M \langle r^{-3} \rangle (f_{yz-zx} - f_{yz+zx})$, respectively, while $H_{\rm cp}$ is written by $H_{\rm cp} = -\kappa \langle r^{-3} \rangle M$. We compare these equations with the experimental data after subtracting the values of $H_{\rm D}^{\rm ax}$ and $H_{\rm D}^{\rm aniso}$ mentioned above and the $H_{\rm STH}$ value, which is calculated by assuming $B = 14.6$–45.8 kOe/$\mu_{\rm B}$ from the B values of the d^2 and d^9 systems,[31,42] from the $H_{\rm n}$ values

TABLE II. Electron occupation number n_j ($j = xy$, $yz \pm zx$) of the $3d_j$ orbital at the Cr sites leading to the CrA–CrD spectra in $K_2Cr_8O_{16}$.

Spectrum	n_{xy}	n_{yz+zx}	n_{yz-zx}
CrA	0.86–0.91	0.74–0.75	0.60–0.65
CrB	0.86–0.91	0.74–0.75	0.60–0.65
CrC	0.85–0.89	0.72–0.73	0.64–0.68
CrD	0.87–0.92	0.72–0.73	0.61–0.65

in Table I. Then we also use $\kappa = 0.5$, which is a typical value for the t_{2g} systems,[33–36,38] and $M = 2.25\mu_B$. We obtain the electron occupation number of the d_j orbital listed in Table II. As seen in Table II, the d_{xy} orbitals at the four Cr sites are predominantly occupied, whereas the $d_{yz\pm zx}$ orbitals are partially occupied, consistent with the band calculation results.[16] This electron configuration leads to a ferromagnetic interaction via the double exchange process for a localized d_{xy} electron and itinerant $d_{yz\pm zx}$ ones as discussed in the previous studies of $K_2Cr_8O_{16}$.[5,16] Also, the electron configurations at the four sites are almost the same, consistent with the experimental result of the synchrotron x-ray-diffraction measurements.[15,16] In spite of such similar electron configurations at the four sites, H_n^{iso} obviously differ from each other among the four sites. This is considered to come from the difference in H_{STH} due to the slight difference in $n_{yz\pm zx}$. The transferred spins from these $d_{yz\pm zx}$ orbitals to the neighboring Cr-4s orbital via the O-2p orbitals can generate the isotropic hyperfine field through a core polarization process of the 4s electron with the coupling constant of $\sim$1200 kOe/μ_B.[46] This large coupling constant leads to the non-negligible difference in H_n^{iso}, even if the difference in $n_{yz\pm zx}$ is slight. Thus, our NMR results of $K_2Cr_8O_{16}$ are understood by the presence of the strong d-p hybridization leading to the Peierls transition model proposed as the mechanism of the MI transition.[15,16]

Finally, it should be noted that the strong hybridization between the double chains in $K_2Cr_8O_{16}$ forms the quasi-1D column composed of the four Cr-O chains where the MI transition takes place due to the Peierls instability.[15,16] This is in contrast to double chain oxides $K_2V_8O_{16}$ and NaV_2O_4 with an edge-shared double chain as a basic electronic structure. Then in $K_2V_8O_{16}$ the MI transition is accompanied by CO,[47–49] whereas the helical magnetic order was shown to appear due to the competition between the FM and AFM interactions in NaV_2O_4.[35] From theoretical studies based on the GGA and GGA + U band calculations, it was shown that the location of the Fermi level in the t_{2g} bands governs the basic electronic properties of the hollandite-type oxides.[5,50] On the other hand, $NaCr_2O_4$, which may have a double chain structure via the corner-shared oxygen as the basic electronic structure, shows the characteristic CMR effect in the AFM phase.[8–10] Thus the strong d-p hybridization is considered to play an important role for the electronic structures and the physical properties of the high-valence Cr oxides with the double chains. Progress of theoretical studies on the STH mechanism is desired to microscopically understand the d-p hybridization in the transition-metal oxides with t_{2g} electrons in the CT region.

V. CONCLUSION

We have made ^{53}Cr NMR measurements to investigate the local electronic structure of $K_2Cr_8O_{16}$. In the ferromagnetic insulating phase, we observed NMR spectra which consist of the four two-dimensional (three-dimensional) powder patterns from the four inequivalent Cr sites at $H = 0$ kOe ($\geqslant$5 kOe). From the analysis of the NMR spectra, we found that the internal fields at the four Cr sites differ from each other in spite of uniform charge densities at the Cr sites. The origin of the difference in the internal field is closely related to the charge-transferred processes which generate supertransferred hyperfine fields. Owing to the strong hybridizations between the Cr-3d and O-2p orbitals, $K_2Cr_8O_{16}$ exhibits peculiar magnetism and transport properties such as the ferromagnetic transition, the metal-insulator transition, and the anomalous hyperfine field.

ACKNOWLEDGMENTS

The authors would like to thank Y. Ohta and Y. Kobayashi for fruitful discussion. This study was supported by the Grant-in-Aid for Scientific Research on Priority Area "Novel State of Matter Induced by Frustration" (Grant No. 22014006) from the Ministry of Education, Culture, Sports, Science, and Technology of Japan, and also the Grants-in-Aid for Scientific Research (Grants No. 24340080 and No. 25610092) from the Japan Society for the Promotion of Science (JSPS). One of the authors, H. Takeda, was also supported by the Program for Leading Graduate Schools entitled "Integrative Graduate Education and Research Program in Green Natural Sciences" and the Grant-in-Aid for JSPS Fellows.

[1] M. Imada, A. Fujimori, and Y. Tokura, Rev. Mod. Phys. **70**, 1039 (1998).
[2] D. I. Khomskii, Lith. J. Phys. **37**, 65 (1997); see also arXiv:cond–mat/0101164 and references therein.
[3] M. A. Korotin, V. I. Anisimov, D. I. Khomskii, and G. A. Sawatzky, Phys. Rev. Lett. **80**, 4305 (1998).
[4] A. Toropova, G. Kotliar, S. Y. Savrasov, and V. S. Oudovenko, Phys. Rev. B **71**, 172403 (2005).
[5] M. Sakamaki, T. Konishi, and Y. Ohta, Phys. Rev. B **80**, 024416 (2009).
[6] G. Kotliar, S. Y. Savrasov, K. Haule, V. S. Oudovenko, O. Parcollet, and C. A. Marianetti, Rev. Mod. Phys. **78**, 865 (2006).
[7] T. R. McGuire, E. J. Scott, and F. H. Grannis, Phys. Rev. **102**, 1000 (1956).
[8] H. Sakurai, T. Kolodiazhnyi, Y. Mihiue, E. Takayama-Muromachi, Y. Tanabe, and H. Kikuchi, Angew. Chem. Int. Ed. **51**, 6653 (2012).
[9] T. Kolodiazhnyi and H. Sakurai, J. Appl. Phys. **113**, 224109 (2013).
[10] H. Takeda, Y. Shimizu, M. Itoh, H. Sakurai, and E. Takayama-Muromachi, J. Korean Phys. Soc. **62**, 1914 (2013).

[11]O. Tamada, N. Yamamoto, T. Mori, and T. Endo, J. Solid State Chem. **126**, 1 (1996).
[12]J. Sugiyama, H. Nozaki, M. Mansson, K. Prsa, D. Andreica, A. Amato, M. Isobe, and Y. Ueda, Phys. Rev. B **85**, 214407 (2012).
[13]K. Hasegawa, M. Isobe, T. Yamauchi, H. Ueda, J. I. Yamaura, H. Gotou, T. Yagi, H. Sato, and Y. Ueda, Phys. Rev. Lett. **103**, 146403 (2009).
[14]P. Mahadevan, A. Kumar, D. Choudhury, and D. D. Sarma, Phys. Rev. Lett. **104**, 256401 (2010).
[15]A. Nakao, Y. Yamaki, H. Nakao, Y. Murakami, K. Hasegawa, M. Isobe, and Y. Ueda, J. Phys. Soc. Jpn. **81**, 054710 (2012).
[16]T. Toriyama, A. Nakao, Y. Yamaki, H. Nakao, Y. Murakami, K. Hasegawa, M. Isobe, Y. Ueda, A. V. Ushakov, D. I. Khomskii, S. V. Streltsov, T. Konishi, and Y. Ohta, Phys. Rev. Lett. **107**, 266402 (2011).
[17]A. Urushibara, Y. Moritomo, T. Arima, A. Asamitsu, G. Kido, and Y. Tokura, Phys. Rev. B **51**, 14103 (1995).
[18]A. Durán, A. Arévalo-López, E. Castillo-Martínez, M. García-Guaderrama, E. Moran, M. Cruz, F. Fernández, and M. Alario-Franco, J. Solid State Chem. **183**, 1863 (2010).
[19]C. P. Slichter, *Principles of Magnetic Resonance* (Springer-Verlag, Berlin, 1990).
[20] A. C. Gossard and A. M. Portis, Phys. Rev. Lett. **3**, 164 (1959).
[21]H. Nishihara, T. Tsuda, A. Hirai, and T. Shinjo, J. Phys. Soc. Jpn. **32**, 85 (1972).
[22]J. H. Shim, S. Lee, J. Dho, and D.-H. Kim, Phys. Rev. Lett. **99**, 057209 (2007).
[23]D. L. Cowan and L. W. Anderson, Phys. Rev. **135**, A1046 (1964).
[24]L. J. Bruner, J. I. Budnick, and R. J. Blume, Phys. Rev. **121**, 83 (1961).
[25]J. F. Baugher, P. C. Taylor, T. Oja, and P. J. Bray, J. Chem. Phys. **50**, 4914 (1969).
[26]A. Narath, Phys. Rev. **140**, A854 (1965).
[27]E. Jedryka, S. Nadolski, and M. Wojcik, J. Magn. Magn. Mat. **40**, 303 (1984).
[28]R. M. White, *Quantum Theory of Magnetism* (Springer-Verlag, Berlin, 1983).
[29]M. Rubinstein, G. H. Stauss, and J. J. Krebs, Phys. Lett. **12**, 302 (1964).
[30]F. Mila and T. M. Rice, Physica C **157**, 561 (1989).
[31]T. Shimizu, H. Yasuoka, T. Tsuda, K. Koga, and Y. Ueda, Bull. Mag. Res. **12**, 39 (1990).
[32]T. Ohama, H. Yasuoka, M. Isobe, and Y. Ueda, J. Phys. Soc. Jpn. **66**, 3008 (1997).
[33]Y. Shimizu, H. Takeda, M. Tanaka, M. Itoh, S. Niitaka, and H. Takagi, Nature Commun. **3**, 981 (2012).
[34]Y. Shimizu, K. Matsudaira, M. Itoh, T. Kajita, and T. Katsufuji, Phys. Rev. B **84**, 064421 (2011).
[35]H. Takeda, M. Itoh, and H. Sakurai, Phys. Rev. B **86**, 174405 (2012).
[36]T. Kiyama, T. Shiraoka, M. Itoh, L. Kano, H. Ichikawa, and J. Akimitsu, Phys. Rev. B **73**, 184422 (2006).
[37]G. P. Singh and S. Ram, J. Mag. Mag. Mater. **322**, 1484 (2010).
[38]T. Kiyama and M. Itoh, Phys. Rev. Lett. **91**, 167202 (2003).
[39]A. Abragam and F. Bleany, *Electron Paramagnetic Resonance of Transition Ions* (Clarendon, Oxford, 1970).
[40]A. J. Freeman and R. E. Watoson, *Hyperfine Interaction* (Academic Press, New York, 1967).
[41]E. Šimánek and Z. Šroubek, *Electron Paramagnetic Resonance* (Plenum, New York, 1972).
[42]J. Kikuchi, H. Yasuoka, Y. Kokubo, Y. Ueda, and T. Ohtani, J. Phys. Soc. Jpn. **65**, 2655 (1996).
[43]F. van der Woude and G. A. Sawatzky, Phys. Rev. B **4**, 3159 (1971).
[44]A. S. Moskvin, N. S. Ovanesyan, and V. A. Trukhtanov, Hyperfine Interact. **3**, 429 (1977).
[45]I. A. Presniakov, V. S. Rusakov, G. Demazeau, A. V. Sobolev, Ya. S. Glazkova, T. V. Gubaidulina, A. M. Gapochka, O. S. Volkova, and A. N. Vasiliev, Phys. Rev. B **85**, 024406 (2012).
[46]A. K. Koh and D. F. Miller, At. Data Nucl. Data Tables **33**, 253 (1985).
[47]M. Isobe, S. Koishi, N. Kouno, J. Yamaura, T. Yamauchi, H. Ueda, H. Gotou, T. Yagi, and Y. Ueda, J. Phys. Soc. Jpn. **75**, 073801 (2006).
[48]Y. Shimizu, K. Okai, M. Itoh, M. Isobe, J-I. Yamaura, T. Yamauchi, and Y. Ueda, Phys. Rev. B **83**, 155111 (2011).
[49]A. C. Komarek, M. Isobe, J. Hemberger, D. Meier, T. Lorenz, D. Trots, A. Cervellino, M. T. Fernandez-Diaz, Y. Ueda, and M. Braden, Phys. Rev. Lett. **107**, 027201 (2011).
[50]M. Sakamaki, S. Horiuchi, T. Konishi, and Y. Ohta, arXiv:0811.4338.